JOURNAL OF MATERIALS SCIENCE 27 (1992) 4247–4260

Characterization of the hot-working behaviour of a P/M Al–20Si–7.5Ni–3Cu–1Mg alloy by hot torsion

J. ZHOU, J. DUSZCZYK, B. M. KOREVAAR
Laboratory for Materials Science, Delft University of Technology, Rotterdamseweg 137, 2628 AL Delft, The Netherlands

B. VERLINDEN
Department of Metallurgy and Materials Engineering, Katholieke Universiteit Leuven, de Croylaan 2, 3001 Heverlee, Belgium

Hot torsion tests were performed to investigate the mechanical and microstructural responses of a quinary Al–20Si–7.5 Ni–3Cu–1 Mg (wt %) alloy, consolidated from a rapidly solidified powder, to deformation at varying temperatures and strain rates. It was found that, under most of the deformation conditions applied, stress–strain curves were characterized by distinct stress peaks, which are usually absent from the curves shown by conventional aluminium alloys. Temperature and strain rate strongly influenced the stress and ductility of the material. Their combined influence on the peak stress has been expressed with a hyperbolic sine equation. The material also exhibited an extraordinarily high strain rate sensitivity, m, and a large m value variation with temperature. A relatively high value of activation energy for deformation was determined, which clearly reflects additional thermal barriers to metal flow, arising from a high volume fraction of multi-phase particles dispersed in the material. Additionally, the microstructure developed in the course of deformation was examined, which showed evidence of the co-operation of dynamic recovery and recrystallization. The initiation of local dynamic recrystallization is a result of a low level of dynamic recovery achievable in the material, which is again different from conventional aluminium alloys.

1. Introduction

Since the middle 1980s, much effort has been made to replace ingot casting with diverse techniques of rapid solidification in fabricating hypereutectic Al–Si-based alloys. Some attempts have been successful in laboratory research and commercial application. At present, many of the alloys are fabricated by atomization as a convenient means of rapid solidification, followed by hot extrusion as an integrated process of consolidation and forming. They are then subjected to a secondary forming process such as forging to shape the extruded materials into the configurations suitable for the components in automotive engines and compressors [1]. Understanding the deformation behaviour and accompanying structural changes of the alloys produced through the powder metallurgy (P/M) route is, therefore, of great importance for determining an appropriate hot-working condition to be applied in fabrication. Very little attention has, however, been paid to developing the forming technology of these alloys, although a large number of hot-worked components are currently used in the automotive industry and multiplication of their production is potentially needed to extend the utilization of the alloys to other industries [2]. Only a few investigations [3–7] have, so far, been carried out on the characterization of the hot-working behaviour of these alloys; notwithstanding, these investigations unanimously show that the hot-working behaviour of the rapidly solidified P/M Al–Si-based alloys is quite different from that of conventional aluminium alloys, owing to the exceptionally heavy alloying and the adoption of the specific fabrication techniques. Unfortunately, because the testing techniques used have been restricted to uniaxial tension, compression and extrusion, each of which has some inherent shortcomings, the workability of the P/M Al–Si-based alloys has not been satisfactorily understood.

A preceding investigation on an Al–20Si–7.5Ni–3Cu–1Mg (wt %) alloy has been performed in an attempt to understand the extrusion behaviour of this technical alloy, initially in the form of an atomized powder [8]. It has, however, been recognized that in extrusion the effective flow stress of the material is not directly measurable and its dependence upon such basic process variables as temperature, reduction ratio and ram speed is hidden in extrusion pressure. Moreover, strain rate, as a combined function of reduction ratio and ram speed, is very non-uniform across a transverse section in the deformation zone, although

0022–2461

mean values can be approximated with the help of plasticity theories. In such a case, a constitutive equation describing the relationship between deformation conditions and the flow stress of the alloy is difficult to establish. Clearly, workability cannot be directly and reliably determined by extrusion alone. Performing simulative tests, as an indirect approach, is necessary to acquire such material properties as flow stress, strain rate sensitivity and activation energy for deformation, so as to correlate the stress of the material with deformation conditions.

Hot torsion is one of the methods that can be used for simulative tests to determine hot workability. In comparison with the other methods like compression and tension, it has the advantage of covering a wide range of strain rates, which can reach those used in practical forming processes such as extrusion and forging. Moreover, in hot torsion, a large strain before the onset of fracture or geometric instability is usually obtainable, which is essential for the tests on the present alloy being brittle in nature. Hot torsion tests were, therefore, chosen for a further investigation on the Al–20Si–7.5Ni–3Cu–1Mg alloy. It aimed at determining the hot-working characteristics of the material over a range of temperatures and strain rates, obtaining the material parameters for establishing a constitutive equation, and examining the microstructures developed during deformation.

It should be pointed out that because the material subjected to hot torsion has already been consolidated from powder by hot extrusion, its deformation behaviour exhibited in the simulative tests cannot be expected to be exactly the same as that in the extrusion of the powder (on which tests cannot possibly be performed). Hot torsion tests can, nevertheless, provide basic information on its workability, which is currently not available because the material with a similar composition, produced by ingot casting, has an extremely low deformability. The information obtained is required to serve as an important guide to the secondary forming and also to the extrusion, though some adjustments may be necessary. It is also worth noting that, while the material in torsion tests has been consolidated, its mechanical behaviour and structural evolution will not be identical to that produced by the conventionl fabrication techniques. This is because many structural features, originated from the rapidly solidified powder, are inherited by the consolidated material, such as fine grain sizes, fine dispersed-phase sizes and broken powder particle boundaries. The specific processing history of the material will inevitably be reflected in its mechanical and microstructural responses to torsional deformation. A point made above is that the material in hot torsion is different from, but still related to that in powder extrusion.

2. Experimental procedure

2.1. Material

The alloy, with a nominal composition (wt %) of 20 Si, 7.5 Ni, 3 Cu, 1 Mg and balance aluminium, was supplied (by Showa Denko K. K., Japan) in the form of an air-atomized powder with a mass median size of 65 μm [9]. The powder was consolidated using hot extrusion at a temperature of 375 °C, a reduction ratio of 20:1, and a ram speed of 5 mm s^{-1}. The extruded rods with a diameter of 11.2 mm were machined into cylindrical torsion specimens with their longitudinal axes parallel to the extrusion direction, and with a gauge length and diameter of 20 mm and 5 mm, respectively. The extruded material to be tested was subjected to thermal and X-ray diffraction analyses, which showed that an equilibrium state was nearly attained in the consolidated material. Therefore, the superimposition of additional structural changes induced by torsional deformation should be minimized.

2.2. Torsion tests

The tests were carried out on a computer-controlled torsion machine, which has been described in detail elsewhere [10]. In the present experiments, the specimens were quickly heated in air by a high-frequency induction coil and consistently soaked for 5 min at testing temperatures to allow temperature stabilization before torsional deformation. This scheme was proven to be applicable, because increasingly prolonged soaking up to 480 min did not yield noticeable differences in the deformation behaviour of the material. The temperature range used was between 350 and 450 °C, which was considered to correspond well to that normally used in hot working of the material. Over this range, sufficient softening can be acquired for easy forming and also the necessary temperature margin below incipient melting at 520 °C is allowed for deformational heating. The testing temperature was controlled by an infrared pyrometer. Before testing, careful adjustment of the heating coil and calibration of the pyrometer were made to minimize temperature non-uniformity along the gauge length of the specimens and to ensure precise measurements of temperature. Three twist rates, $\dot{\theta} = 11$, 110 and 330 rev min^{-1}, were applied, which produced the strain rates, $\dot{\varepsilon} = 0.083$, 0.83 and 2.49 s^{-1} at the specimen surface, equivalent to those in uniaxial compression or tension (for simplicity the equivalent strain rates at the specimen surface are termed as strain rates hereafter). During testing, a constant geometry of the specimens was maintained by constraining their elongation in the axial direction, and the developed axial force was measured, which consistently showed negligibly low values.

In the present work, the tests were divided into two series to investigate the mechanical behaviour and microstructural development of the material during torsional deformation. In the first series, deformation was performed to fracture. The recorded torque M (Nm)–twist θ (rev) curves were converted into stress σ–strain ε curves, equivalent to those in uniaxial compression or tension, using the following equations [11]:

$$\sigma = 3^{1/2} M (3 + m + N)(2\pi r^3)^{-1} \quad (1)$$

$$\varepsilon = 3^{-1/2} 2\pi r \theta l^{-1} \quad (2)$$

where r and l are the gauge radius and gauge length of

the specimens, respectively, and m and N are strain rate sensitivity and work-hardening rate, respectively, given by

$$m = (\partial \ln M/\partial \ln \dot{\varepsilon})_{\varepsilon,T} \quad (3)$$

$$N = (\partial \ln M/\partial \ln \varepsilon)_{\dot{\varepsilon},T} \quad (4)$$

In the second series, the specimens were deformed at the temperature of 400 °C and strain rates of 0.083 and 2.5 s^{-1}. Deformation was interrupted at a number of desired strains and then the deformed specimens were immediately quenched (within 1 s) by a water sprayer to retain the as-worked microstructures developed in the material.

2.3. Microscopy

The microstructures of the material having undergone the second series of tests were examined using a Philips 400T transmission electron microscope (TEM) working at 120 kV. Slices were cut at 0.5 mm below the surface (normal to the radius) in the central region of the gauge section. They were finally thinned with an ion mill operating at a beam current of 0.5 mA.

3. Results and discussion

3.1. Stress–strain curves

Fig. 1a and b show representative stress–strain curves which are converted, by using Equations 1 and 2, from the corresponding torque–twist curves obtained from the tests at different twist rates and temperatures. It was generally observed that, after having been work hardened at the initial stage of deformation, the material exhibited a distinct stress peak followed by considerable softening, particularly at low temperatures and high strain rates. Only at the strain rate of 0.083 s^{-1} and temperatures of 425–450 °C, was the characteristic stress peak flattened (Fig. 1b). It was also noticed that the degree of softening beyond the stress peak depended on the temperature and strain rate applied, being higher at lower temperatures and higher strain rates. The alteration of dominance from work hardening to softening is the most notable characteristic of the curves obtained from the tests. This deformation behaviour is not often observable in tests on conventional aluminium alloys, which normally display a gradual increase and then a plateau in stress until fracture, as a consequence of the balance between work hardening and softening by dynamic recovery [12]. It has, however, been encountered in torsion tests on several aluminium alloys. Basically, a distinct stress peak is indicative of the occurrence of softening by dynamic recrystallization during deformation. However, this softening mechanism usually does not operate in aluminium alloys with high stacking fault energies, which enable dislocations to cross-slip and climb easily so that full dynamic recovery can occur. To explain the observed stress peak, a variety of terms, specific to individual alloys and their states in processing, has been utilized [13], though firm structural evidence to support the explanations is often difficult to obtain. The appearance of the stress peak in the tests on the present material may be ascribed to the following effects.

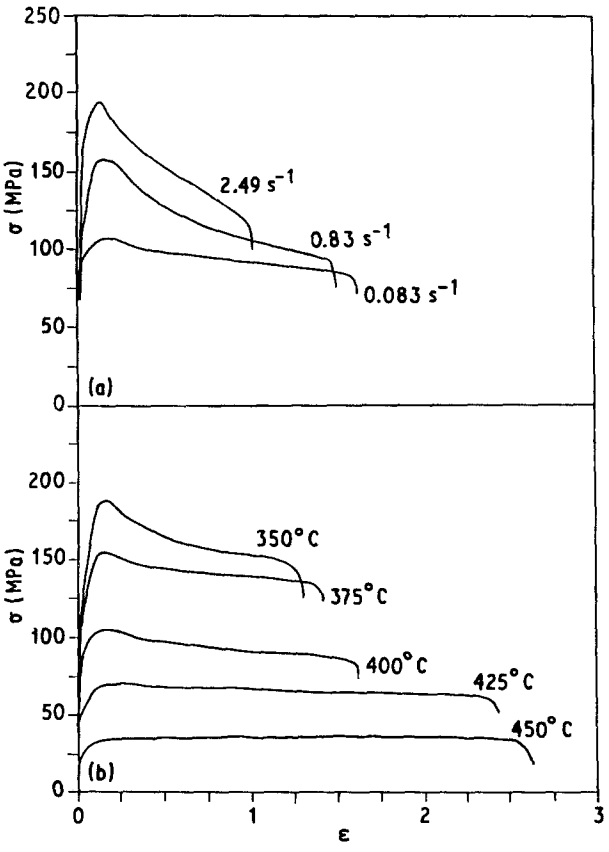

Figure 1 A selection of the equivalent stress–strain curves obtained from torsion tests at (a) a temperature of 400 °C, and (b) a low strain rate of 0.083 s^{-1}.

(i) Dynamic recrystallization. The shape of the flow curves, exhibited by the present material, is not completely the same as that shown by copper and nickel alloys which have lower stacking fault energies and restore predominantly by dynamic recrystallization. It is, however, almost identical to the shape observed in torsion tests on an Al–5Mg–0.8Mn alloy, which has been proved to restore by both dynamic recovery and dynamic recrystallization [14]. The occurrence of local dynamic recrystallization in the present material has been observed during extrusion [8], and also during torsional deformation, as will be shown later in conjunction with the as-deformed microstructures. This gives evidence that this effect bears the primary responsibility for the observed stress peaks. Because a widespread operation of the dynamic recrystallization mechanism did not occur in the material, the shape of the stress–strain curves appeared to be a little different from that shown by copper and nickel alloys, and to be sensitive to the strain rate and temperature applied. For example, the characteristic peaks disappeared at the low strain rate of 0.083 s^{-1} and high temperatures of 425–450 °C (see Fig. 1b). Under these conditions, the stress–strain curves appeared to be typical of a material that restores only by dynamic recovery, work hardening followed by steady-state deformation. This may be because, for dynamic recrystallization to occur, high concentrations of stresses (high-density dislocations) are necessary for the nucleation of new crystals. At the high temperatures and low deformation rate, dynamic recovery, mainly controlled by

diffusion, will decrease the internal stresses sufficiently to prevent the nucleation for recrystallization and thus dynamic recovery can be the only operating softening mechanism. At the lower temperatures and higher strain rates, however, the stress concentrations in the material can be built up to sufficient heights to cause nucleation of the recrystallization because of the relatively slow recovery under these conditions. At a given temperature and with the increase of strain rate, softening by dynamic recrystallization becomes increasingly important, as indicated by the sharpening stress peaks in Fig. 1a. At the low temperatures of 350–375 °C and high strain rates, dynamic recrystallization may be assisted by Effect (ii).

(ii) Temperature rise, resulting from deformational heating. This effect leads to thermal softening in the gauge section, particularly at high strain rates because the deformation under those conditions approaches an adiabatic process. As the peak stress of the present material was found to be strongly temperature dependent, which will be discussed later on, a small increase in temperature could measurably lower this stress. However, the temperature variation recorded in the entire course of deformation indicated that, when strain rates were not too high, the temperature rise was insignificant. Hence, this effect is unlikely to be fully responsible for the observed stress peaks shown under all testing conditions. This argument is supported by the fact that, in the tests at the low strain rate of 0.083 s^{-1} when deformational heating would be of minor importance, the stress peaks were also observed at the testing temperatures of 350–400 °C, as shown in Fig. 1b. This suggests that other effects, e.g. Effect (iii), might also be involved.

(iii) Structural changes occurring during deformation, such as precipitation, transformation and second-phase coarsening. X-ray diffractometry revealed little change in the aluminium matrix lattice parameter and phase constituents of the material during the tests, indicating that significant strain-induced precipitation or transformation did not occur. Even if there was some undetectable precipitation, it would be very unlikely to have such a marked impact on the flow behaviour of the material, because a loss in solutes would be balanced by an increase in precipitate density [15]. Coarsening of second-phase particles is, however, a possibility, which has been considered to be responsible for the stress peak exhibited by a 2024 alloy in torsion [16, 17]. Among the constituent phases dispersed in the aluminium matrix of the present material, the Mg_2Si phase has a tendency to coalescence, while the others (silicon crystals, Al_3Ni, $Al_3(NiCu)_2$, and Al_7Cu_4Ni) have shown to be thermally stable at the testing temperatures [8, 18]. Hence, the coarsening of the Mg_2Si phase might be relevant to the observed peak, but this could not microscopically be ascertained in the current work. Moreover, the coarsening, which should be enhanced at a high testing temperature and permitted at a low strain rate, cannot fully account for the flattening of the stress peak at the strain rate of 0.083 s^{-1} and temperatures of 425–450 °C.

On the basis of the above considerations, it is plausible to infer that these three effects worked together to result in softening beyond the stress peak, as shown in Fig. 1. Among these effects, dynamic recrystallization is likely to be the principal contributor.

Another important characteristic of the stress–strain curves was the very slight variation of the strain to the stress peak with temperature and strain rate. This is in contrast with the usual observation that the strain to the stress peak decreases progressively with rising temperature and decreasing strain rate [14]. If the observed stress peak is attributed mainly to the occurrence of dynamic recrystallization in the material, this strain should be representative of a critical value for the onset of this softening mechanism, which is thermally activated and strain and strain-rate controlled. In this sense, it should appear at a lower strain when temperature is higher and strain rate lower. The presently observed low sensitivity of this strain to temperature may be due to the existence of two additional factors in the material, as discussed earlier, that, with the decrease of temperature, dynamic recrystallization and deformational heating become increasingly important. These two factors will affect the usual variation of the strain to the peak with temperature. Temperature rise converted from strain energy is likely to be responsible for the slight variation of this strain with strain rate. At a high strain rate, deformational heating would promote the onset of dynamic recrystallization. Such a disturbing effect of temperature rise on the strain to the stress peak at a high strain rate has also been observed in torsion tests on Cu–P alloys [19]. This result thus seems to confirm the involvement of temperature rise in torsional deformation, which has been considered to be partly responsible for the softening at high strain rates, as discussed earlier.

The ductility of the material was found to be very low in comparison with that of conventional aluminium alloys. At low temperatures and high strain rates, a steady state of deformation could not be attained before failure, as shown in Fig. 1a. Extensive steady-state metal flow was only possible at relatively low strain rates (Fig. 1b), indicating a decisive effect of strain rate on the achievable ductility. Fig. 2 shows the variation of the strain to fracture, ε_f, with temperature and strain rate, which has the same trend as that exhibited by other aluminium alloys. The increase of ε_f at a higher temperature and a lower strain rate is primarily due to reduced stress concentrations at triple points and at second-phase particles where the initiation and propagation of micro-cracks take place. Such a trend has been regarded as an indication that dynamic recovery is a principal restoration mechanism in aluminium alloys, because for the dynamically recrystallized materials the variation of ε_f with strain rate has an opposite trend that ε_f increases with rising strain rate [20]. In this sense, the present results would suggest that dynamic recrystallization is not the major restoration mode in the alloy, but a mechanism supplementary to dynamic recovery, as in an Al–5Mg–0.8Mn alloy [14]. It is, however, worth noting the ductility of an aluminium alloy is dependent not only upon restoration mechanisms but also upon

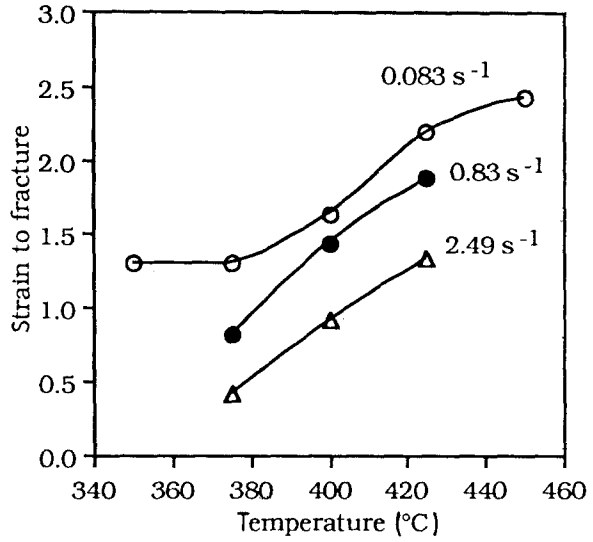

Figure 2 The strain to fracture at different temperatures and surface equivalent strain rates.

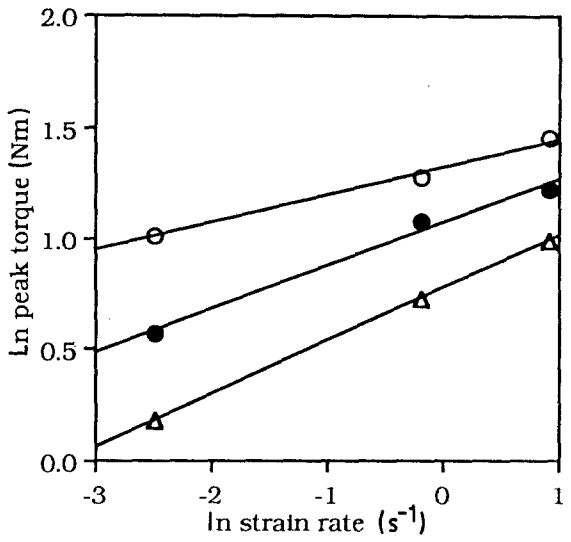

Figure 3 Determination of strain rate sensitivity at different temperatures.

fracture mechanisms. In the present alloy, fracture initiates by the cracking of block-like silicon crystals and the decohesion between the aluminium and dispersed-phase particles (silicon crystals and nickel-containing dispersoids) [21], which are enhanced by deformation at a higher rate. Note that the total volume fraction of the dispersed-phase particles with various sizes in the aluminium matrix of the material is nearly 30%, which gives a very high interfacial area and an easy path to the linkage of micro-cracks. If an increased density of recrystallization nuclei, resulting from deformation at a higher strain rate, could not cope with the enhanced decohesion, the material would fail at an earlier stage of deformation, even during the softening before reaching the steady-state deformation, as indeed observed in the present experiments (see Fig. 1a).

3.2. Strain rate sensitivity

Fig. 3 shows plots of the peak torque against strain rate to derive the strain rate sensitivity, as defined by Equation 3, of the material: $m = 0.13$ at 375 °C, 0.20 at 400 °C and 0.24 at 425 °C. These m values are apparently very high in comparison with those of various grades of conventional aluminium alloys ($m = 0.026$–0.227 at 300–500 °C) [22], but in good agreement with those determined by using tensile, extrusion and compressive tests on other hypereutectic Al–Si-based alloys produced by powder metallurgy [4, 6, 7]. The high m values mean that the material can be strain-rate hardened. A practical implication of this result is that a reduction in deformation rate (for example, ram speed in extrusion) can considerably reduce the flow stress of the material so that a reduced temperature or an increased strain can be applied. As a high deformation rate is usually desirable in commercial production for economic reasons, an adjustment of process parameters (temperature, strain, and strain rate) is necessary in deforming the present material, being different from conventional aluminium alloys which are much less strain-rate sensitive. The definite relationships between the m values and the structure of the material are at present uncertain, and thus a satisfactory explanation of the high m values is difficult to give. Nevertheless, one of the causes may be the presence of a high volume fraction of silicon crystal phase (nearly 20%) in the material, which has a linear thermal expansion coefficient about one-eighth of aluminium, thereby imposing stresses on the neighbouring aluminium matrix when the material is heated up to the testing temperatures. It has been experimentally observed that the imposed random internal stresses would assist the plastic flow of the aluminium matrix and lead to a low stress exponent and a high strain rate sensitivity, particularly when applied stresses are low [23]. The enhancement of the m value may be due to an increase of the resistance to instability of metal flow, resulting from the pre-existing stresses, if the m value is regarded as a measure of the capacity of a material to resist plastic instability [24]. This observation has been utilized as a principle to enhance the m value of an aluminium alloy and to obtain superplasticity by adding silicon carbide whiskers and exercising thermal cycles. Therefore, the stresses imposed by the silicon crystals are likely to be relevant to the high m values of the material, as consistently found in other Al–Si alloys [4, 6, 7, 25]. The other possible causes for the high m values will be discussed below at some length.

In unravelling the complicated nature of the m value, it may be more convenient to consider the steady-state deformation involving a single restoration mechanism, for which the correlations among microstructural parameters, mechanical properties and deformation conditions are relatively well established. For the present alloy, though localized dynamic recrystallization occurred during deformation, dynamic recovery might still be regarded as the major restoration mechanism, which is mainly governed by vacancy movement under applied stresses. To consider the steady-state deformation, the m values at the strain $\varepsilon = 0.5$ were determined in the way analogous to Fig. 3, because the strain rate sensitivity is a

function of strain in addition to temperature and strain rate. The m values of 0.11 at 375 °C, 0.16 at 400 °C, and 0.18 at 425 °C were obtained. It is apparent that, though being generally lower than the m-values determined at the stress peak, the m values at $\varepsilon = 0.5$ (which is in or near the steady state of deformation) remain high as compared with those of conventional aluminium alloys [22] and have the same trend to the variation of temperature as that of the m values determined at the stress peak. It is generally accepted that, in the steady-state deformation controlled by atomic diffusion, the strain rate $\dot{\varepsilon}$, and stress, σ, obey the following semi-empirical relationship [25]

$$\dot{\varepsilon} = (AG\boldsymbol{b}/kT)(\boldsymbol{b}/d)^p(\sigma/G)^n D \quad (5)$$

in which A is a dimensionless constant, G the shear modulus, $\boldsymbol{b}$ the Burgers vector, k the Boltzmann constant, T the absolute temperature, d the grain size, p the grain size exponent, n the stress exponent ($= 1/m$), and D the diffusion coefficient given by

$$D = D_0 \exp(-\Delta H/RT) \quad (6)$$

where D_0 is a frequency factor, ΔH the activation energy, and R the universal gas constant. We may reform Equation 5 and combine it with Equation 6, leading to

$$m = (\ln G - \ln\sigma)/(\ln K + \ln D_0 + \ln G - \Delta H/RT - \ln\dot{\varepsilon} - \ln T - p\ln d) \quad (7)$$

in which K is a new constant combining A, $\boldsymbol{b}^{1+p}$ and k. From Equation 7, it can be seen that the m value is a complicated function of both material properties and deformation conditions. As far as the material properties are concerned, the m values are predominantly determined by the activation energy, ΔH, and also affected by the shear modulus, G. For the present alloy, the major recovery mechanisms, dislocation cross-slip and climb, are restricted by a high volume fraction of multi-phase particles, as additional barriers to metal flow so that the other mechanisms such as pinning and unpinning must be operative, which are stress assisted and thermally activated. The activation energy, ΔH, which reflects the overall barriers over which dislocations can move, must be higher than that of pure aluminium, as indeed found and will be given later. Moreover, it has been reported that the present alloy has a relatively high shear modulus which is approximately one-third the Young's modulus (99 000 MPa) [26]. The combined effect of the high activation energy and shear modulus in Equation 7 is, therefore, considered to be largely responsible for the high m values of the material.

Based on the high m values of a hypereutectic Al–Si based alloy produced by powder metallurgy, shown in compressive tests, a possibility of superplasticity was suggested [7]. The present results, however, seem to rule out this possibility, although the obtained m values indeed approach those of superplastic alloys. As presented earlier, the ductility of the material in the torsion tests is consistently low (the highest equivalent strain to fracture is only about 2.5 at 450 °C and 0.083 s^{-1}, as given in Fig. 2, and also note the difference in achievable ductility between torsional and tensile deformation). The low ductility is probably due to the cracking of the dispersed-phase particles and the interfacial decohesion, which act as the major fracture mechanisms [21] and accelerate the failure of the material. The present results appear to give an example that a high strain rate sensitivity is not necessarily associated with a high ductility.

Another interesting feature of the m values of the present material is their very strong temperature dependence. The results show that to double the peak stress of the material requires an increase of strain rate by 18 times at 425 °C ($m = 0.24$) but by 207 times at 375 °C ($m = 0.13$). In other words, the stress of the material can be more effectively reduced by lowering the deformation rate at a higher temperature. A similarly strong m value dependency on temperature has also been reported in Al–Fe and Al–Fe–Co alloys [27]. Over the usual temperature range used for hot working of aluminium alloys (above $T_m = 0.55$ where T_m is the homologous temperature, K), an increase of m value with a rise of temperature is a common observation, but clear explanations cannot be found in the literature currently available. Because Equation 5 appears to link the material properties with deformation conditions, the explanation of the large m value variation with temperature was attempted to resort to this equation, which is at present most commonly used in deformation of metals. It can be seen from Equation 7, reformed from Equation 5, that only the variation of the flow stress is in favour of the desired explanation of the m value increase over 375–425 °C, while the terms in the denominator are essentially unaffected by the small temperature change. Although it has indeed been found that the flow stress of the present alloy decreases greatly with rising temperature, this decrease cannot possibly cause the m value to increase from 0.13 to 0.24 (determined at the stress peak) or from 0.11 to 0.18 (determined at $\varepsilon = 0.5$) in view of Equation 7. In other words, the obtained experimental data fail to be correlated to Equation 5. This suggests that some additional factors, pertinent to temperature, stress and strain rate, should be included in Equation 5, to make it applicable to the deformation of the technical alloy, although this will further complicate the picture. The following factors may be taken into consideration: (i) volume fraction and size of second-phase particles, which directly affect flow stress and structure developed during deformation; (ii) size of subgrains, which is influenced by deformation temperature and varies linearly with the reciprocal σ/G; (iii) dislocation density, which is particularly important for the present alloy in which the degree of dynamic recovery is temperature dependent; and (iv) internal stresses, which are imposed by the second-phase particles. Among these factors, the first factor seems to be indispensable in view of the effect of particles on dislocation motion, which is virtually absent in pure aluminium with its insensitivity of m value to temperature. Basically, strain rate is dependent upon the velocity of dislocations and the latter is, in turn, affected by pinning. At a higher temperature,

move recovery mechanisms such as node unpinning are operative and thus a higher strain rate sensitivity can be expected. This may partly account for the high m value sensitivity to temperature, as consistently found in dispersion-strengthened aluminium alloys [27]. The presence of second-phase particles is also related to the above-mentioned second and third factors, which results in a strong dependence of the degree of dynamic recovery upon temperature. It has been found in an Al–Mg alloy that this enhanced dependence is associated with the high m value sensitivity to temperature [28]. The fourth factor appears to be unique for the present alloy with a high volume fraction of silicon crystals. As discussed earlier, the internal stresses, arising from the difference in thermal expansion coefficient between the silicon crystals and aluminium matrix, reduce the effective stress to drive dislocations. At a higher temperature, the difference between the internal stresses and the applied stress is smaller, which leads to a higher strain-rate sensitivity [29].

3.3. Dependence of stress on temperature and strain rate

With the m values, it was possible to calculate the peak stress of the material at different temperatures and strain rates, by using Equation 1, in which the work-hardening exponent, N, was assumed to be zero, as customarily done for hot-working aluminium alloys. It was observed that the material exhibited a regular decrease in the stress with the rise in temperature, as shown in Fig. 4. This suggests that there were no structural changes occurring over the temperature range, which were capable of specially affecting the peak stress of the material. It was also noted that temperature had an extraordinarily strong influence on the peak stress as compared with conventional aluminium alloys like AA2024 and AA7075 [10]. An important indication obtained from this result is that, for easy forming, an increase in temperature can substantially lower the flow stress of the materia and thus the external force requirement for deformation, provided that it is metallurgically allowed. This strong influence is typical of dispersion-strengthened aluminium alloys which contain dispersed particles pinning dislocations [27, 30]. In the present alloy, the silicon crystals and three nickel-containing dispersoids [8] do not shear at the testing temperatures and thus the motion of dislocations must occur through by-passing these internal particles by the Orowan mechanism that is thermally activated and stress-assisted. At a low temperature, dislocations have difficulty in by-passing them, so that the material has an enhanced resistance to deformation. The result obtained also indicates that at 375 °C the material has a peak strength of 152 MPa at the lowest strain rate, which satisfactorily meets its hot-strength requirements for use in automotive engines and compressors. Additionally, the observed strong influence of temperature on the peak stress explains the softening beyond the stress peak, which is partly caused by a temperature rise, as discussed earlier. This influence is also responsible for a high activation energy for deformation, which will be shown later.

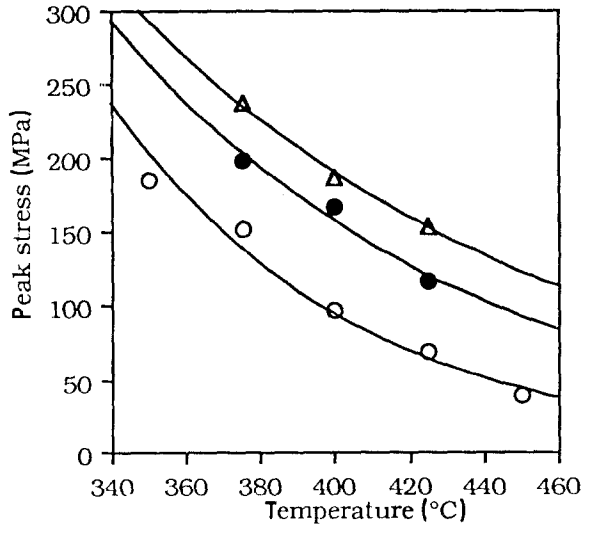

Figure 4 Variation of the peak stress with temperature; surface equivalent strain rates: (○) 0.083 s^{-1}, (●) 0.83 s^{-1}, (△) 2.49 s^{-1}.

Strain rate is another important deformation variable that influences the flow behaviour of a material. It is generally accepted that the deformation behaviour of an aluminium alloy in hot working is similar to that in creep and the correlations between stress, σ, and strain rate, $\dot{\varepsilon}$, can be described by

$$\dot{\varepsilon} = A_1\sigma^n \quad \text{(for low stress)} \tag{8}$$

$$\dot{\varepsilon} = A_2 \exp(\beta\sigma) \quad \text{(for high stress)} \tag{9}$$

or

$$\dot{\varepsilon} = A_3[\sinh(\alpha\sigma)]^{n'} \tag{10}$$

where A_1, A_2 and A_3 are temperature-dependent constants, and α, β, n and n' material constants. It was found that the hyperbolic sine Equation 10 gave the most satisfactory fit to the data presently obtained, and was therefore taken as the basic formula for a constitutive equation suitable for use at various temperatures. To satisfy the requirements that α and n' in Equation 10 are independent of temperature over the experimental range, an attempt was made to plot the logarithmic strain rate against ln $\sinh(\alpha\sigma)$ at the temperatures of 375, 400 and 425 °C (for which the peak stress was again used). The best fit to the parallel straight lines was obtained with the constitutive constants: $\alpha = 0.015\ \text{MPa}^{-1}$ and $n' = 2.46$, see Fig. 5. The linearity in Fig. 5 confirms the validity of Equation 10 empirically describing the relationship between the peak stress and strain rate at a constant temperature.

To establish a constitutive equation, it is necessary to include a temperature factor. For this, the peak stress was first plotted against the reciprocal absolute temperature, which is shown in Fig. 6. The apparent linearity at the different strain rates suggests the incorporation of an Arrhenius energy term in Equation 10, leading to

$$\dot{\varepsilon} = A'[\sinh(\alpha\sigma)]^{n'}\exp(-\Delta H/RT) \tag{11}$$

where A' is a temperature-independent constant. Obviously, to utilize this constitutive equation, it is

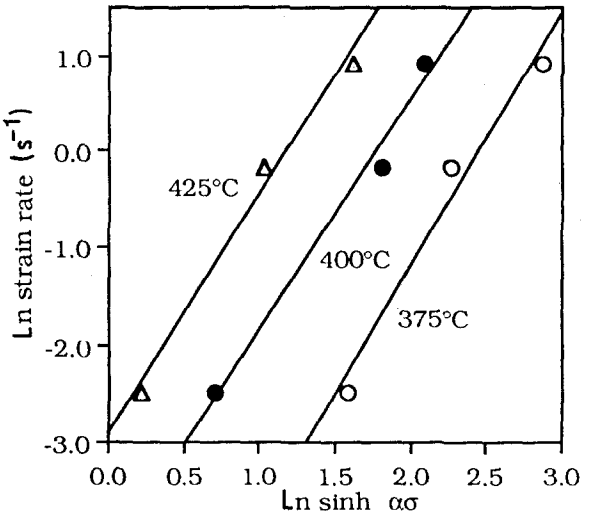

Figure 5 Application of the hyperbolic sine equation at the given temperatures to determine the constitutive constant n' in Equation 10.

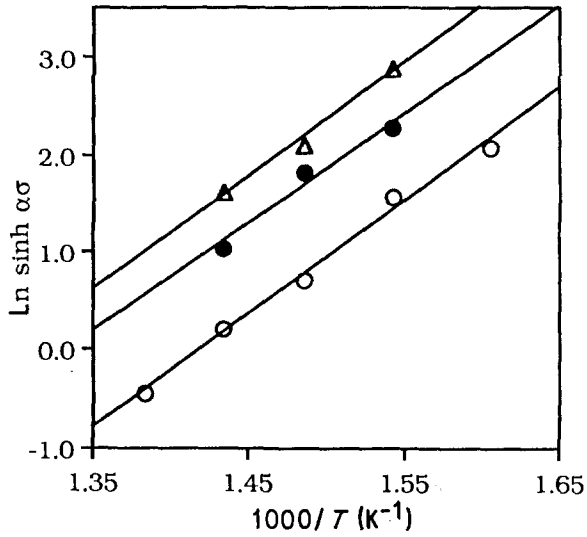

Figure 7 Determination of the activation energy for deformation at the peak stress; surface equivalent strain rates: (○) 0.083 s^{-1}, (●) 0.83 s^{-1}, (△) 2.49 s^{-1}.

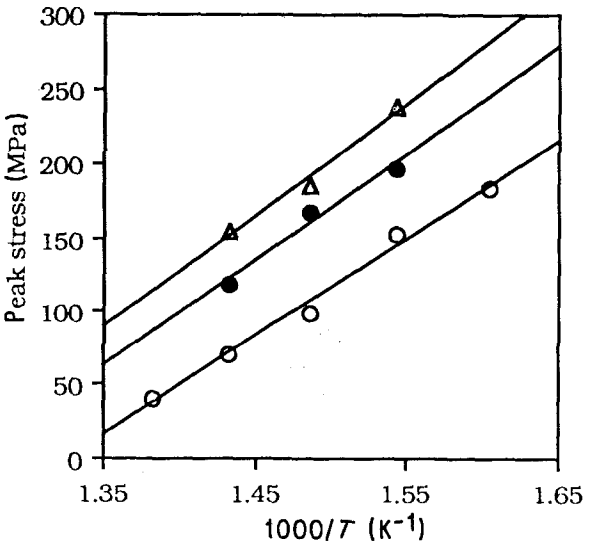

Figure 6 Plot of the peak stress against the reciprocal absolute temperature; surface equivalent strain rates: (○) 0.083 s^{-1}, (●) 0.83 s^{-1}, (△) 2.49 s^{-1}.

necessary to define the activation energy for deformation, ΔH, which can, in theory, be obtained by plotting $\ln \dot{\varepsilon}$ against the reciprocal temperature at a constant flow stress. The slope of the plot is then proportional to ΔH, namely

$$\Delta H = -R(\partial \ln \dot{\varepsilon}/\partial T^{-1})_{\sigma} \quad (12)$$

However, in torsion tests, it was difficult to satisfy the requirement of Equation 12, because a constant flow stress over a range of strain rates was not obtainable. We alternatively rewrote Equation 11 as

$$\ln \sinh(\alpha\sigma) = 1/n'(-\ln A' + \ln \dot{\varepsilon} + \Delta H/RT) \quad (13)$$

With this equation, an average ΔH value of 233 kJ mol^{-1} was derived from the plots shown in Fig. 7 in which the peak stress was used, and so was an average $\ln A'$ value of 37.3. From Equation 13, it is clear that the ΔH value is proportional to the slope of the $\ln \sinh(\alpha\sigma)$ T^{-1} plot, and is thus determined by the variation of the flow stress with temperature. As shown earlier, the material is much stronger at a lower temperature, and thus the slope and ΔH value must be high. Indeed, the ΔH value of the present alloy obtained from the peak stress is much higher than that of commercial-purity aluminium (155 kJ mol^{-1}) [31] which is close to the activation energy for self-diffusion of aluminium (126–142 kJ mol^{-1}) [32]. In the literature, a very wide variation from 116–285 kJ mol^{-1} [28, 30, 33–35] has been reported on the activation energy values of various grades of aluminium alloys in differing states, but no satisfactory explanations of their variation have ever been given, primarily because of their complexity. It is, nevertheless, widely accepted that the ΔH value basically reflects the energy barriers over which deformation can take place. For pure aluminium, the ΔH value is an indicator of the energy barriers for self-diffusion, which largely governs dislocation motion. For aluminium alloys, the ΔH value is affected by solute concentrations in a complicated way, which usually, but not necessarily, act as additional barriers to the free motion of dislocations [36]. For the present heavily alloyed material, a part of the silicon and magnesium added could be resolved in the aluminium matrix at the testing temperatures, which might decrease the stacking fault energy of the matrix, increase the stacking fault width and thus enhance the energy for cross-slip of screw dislocations [37]. The resolution is, however, unlikely to influence the activation energy of the alloy to such a great extent, because a reverse effect is also created by the atomic misfits between the solutes and aluminium matrix, which generate additional vacancies to promote dislocation climb proceeding by a diffusion mechanism. Another factor is the dispersion of second-phase particles. For an Al–Si binary alloy (Al–13Si), the ΔH values of 132–139 kJ mol^{-1} at the stresses of 4–7 MPa have been reported [25]. For an Al–20Si–3Cu–1Mg quaternary alloy, the ΔH values of 145–163 kJ mol^{-1} at the stresses of 80–90 MPa have been determined

using tensile tests [4]. For the present quinary alloy, a ΔH value of 233 kJ mol^{-1} has been obtained at the stresses of 40–238 MPa. These results indicate that, with the increasing complexity in alloying and the accompanied increase in the volume fraction of second-phase particles, the activation energy indeed deviates gradually from that for aluminium self-diffusion which governs the climb of edge dislocations. Such a deviation is understandable, if the interactions between the particles and dislocations are taken into consideration. For the present alloy, silicon crystals and three kinds of nickel-containing dispersoids, nearly insoluble upon heating to the testing temperatures [8], are present, acting as obstacles to the cross-slip and climb of dislocations. To by-pass these obstacles, additional energy is required to close extended dislocations and then allow them to leave their original glide planes, which will undoubtedly increase the ΔH value. An additional factor is that a different softening mode other than dynamic recovery, dynamic recrystallization, is involved in the deformation, which proceeds by grain-boundary movement instead of vacancy movement. It has been stated that when dynamic recrystallization participates in deformation, an increase of the ΔH value by 20% can be expected [14]. The combined effect of the factors, discussed above, would result in the presently derived ΔH value of the material.

So far, we have established a constitutive equation for the deformation of the alloy

$$\dot{\varepsilon} = 1.58 \times 10^{16}[\sinh(0.015\sigma)]^{2.46} \exp[-233\,000/(8.314T)] \quad (14)$$

Although the exact physical significance of each constitutive constant in Equation 11 is rather vague, it is interesting to compare the obtained values in Equation 14 with those of commercial-purity aluminium ($A' = 2.35 \times 10^{10}$ s^{-1}, $\alpha = 0.03$ MPa^{-1}, and $n' = 4$–4.2 [31]) and with those of various grades of conventional aluminium alloys ($A' = 3.45 \times 10^{8}$–3.8×10^{11} s^{-1}, $\alpha = 0.012$–0.037 MPa^{-1}, and $n' = 2.22$–5.3 [38, 39]). If A' is regarded as a frequency factor (proportional to the density of activateable sites) [40], the higher value of the present alloy reflects that more dislocations overcome obstacles to move in unit time. If α is a measure of activation volume [19], the lower value of the present alloy suggests a smaller volume of material participating in a single deformation event, resulting from the restriction by the particles resisting deformation. And if n' is associated with climb-controlled processes, irrespective of dispersed particles, the lower value of the present alloy indicates the existence of viscous drag of solute atmospheres in the material during deformation [28].

As the constitutive Equation 14 was graphically determined, errors would be entailed in the procedure. To check this equation, all the data obtained over the range of temperatures and strain rates were correlated to it. For this, we expressed Equation 11 as the temperature-compensated strain rate, or Zener–Hollomon parameter, Z

$$Z = \dot{\varepsilon}\exp(\Delta H/RT) = A[\sinh(\alpha\sigma)]^{n'} \quad (15)$$

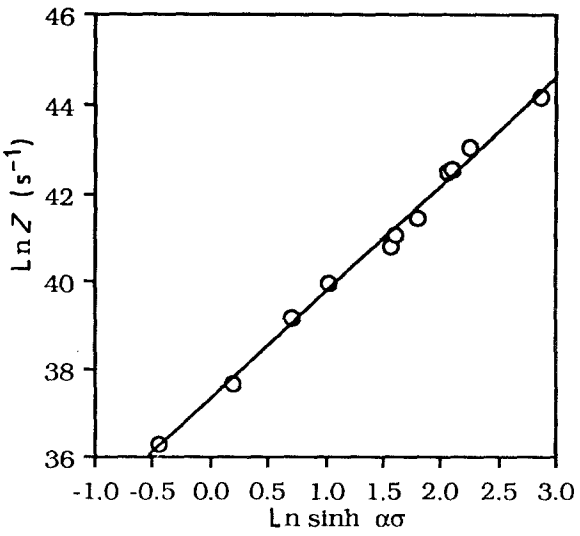

Figure 8 Applicability of the Zener–Hollomon parameter to the torsional deformation.

A single linear relationship between $\ln \dot{\varepsilon}\exp(\Delta H/RT)$ and $\ln[\sinh(\alpha\sigma)]$ was obtained, as shown in Fig. 8. It demonstrates that the constitutive constants, derived from Figs 5 and 7, are not significantly in error (the correlation coefficient for the linear relationship being 0.993). Fig. 8 also verifies that the temperature-compensated strain rate, Z, is applicable to the description of the material properties in relation to deformation conditions. This verification is of great significance for the control of a metal-forming process of the material with the Z parameter.

3.4. Microstructural development during deformation

3.4.1. Low strain rate (0.083 s^{-1})

In the current work, microstructural examination was first carried out on the material in the course of deformation at 400 °C and 0.083 s^{-1}: in the work-hardening regime, at the stress peak, and in the steady-state regime, where deformation was ceased and the as-deformed specimens were water quenched. Fig. 9 shows transmission electron micrographs taken from the material strained to $\varepsilon = 0.068$, which is in the work-hardening regime and at about 50% of the strain to the stress peak. It was observed that at this stage the principal development of microstructure was multiplication of dislocations and formation of subgrains. This development was, however, considerably affected by the existence of massive particles with various sizes in the material (silicon crystals and nickel-containing dispersoids). In most of the regions, a cellular structure formed by dislocation networks was observed, as typically shown in Fig. 9a. At this stage the rate of dislocation generation was far in excess of annihilation. Dislocation density was particularly high in the vicinities of particles, where newly generated dislocations encountered difficulties in moving to compose ordered arrays as cell walls and subgrain boundaries. In the regions less populated with particles, the formation of the subgrains was in progress (see Fig. 9b). The developing subgrains contained a high density of dislocations. The subgrain

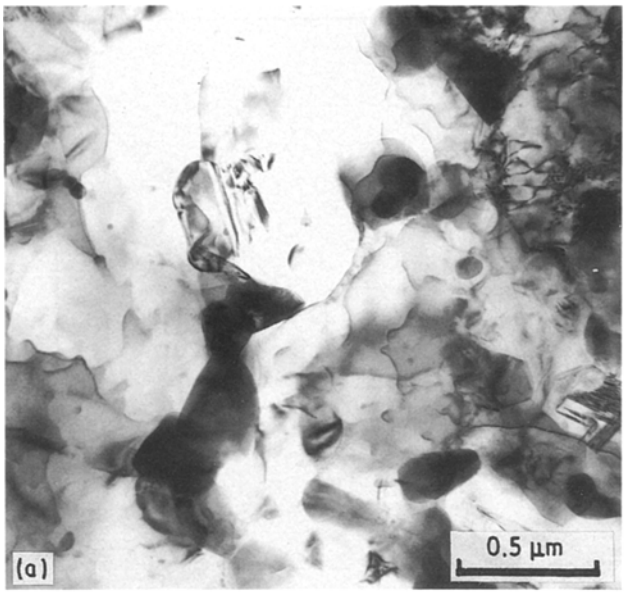

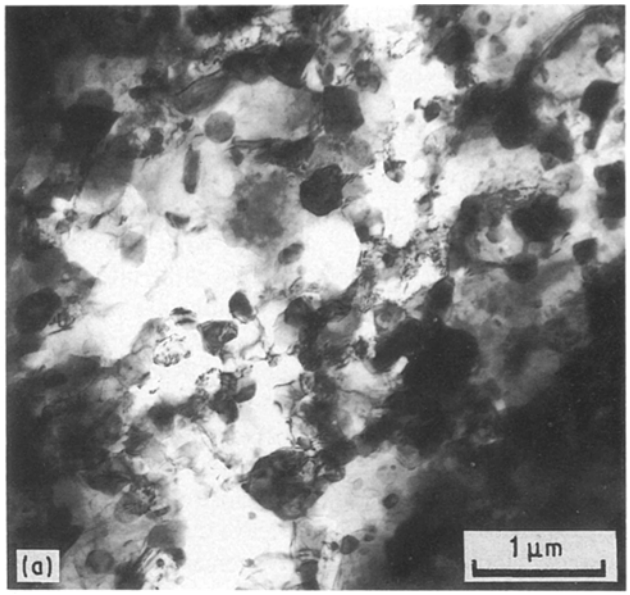

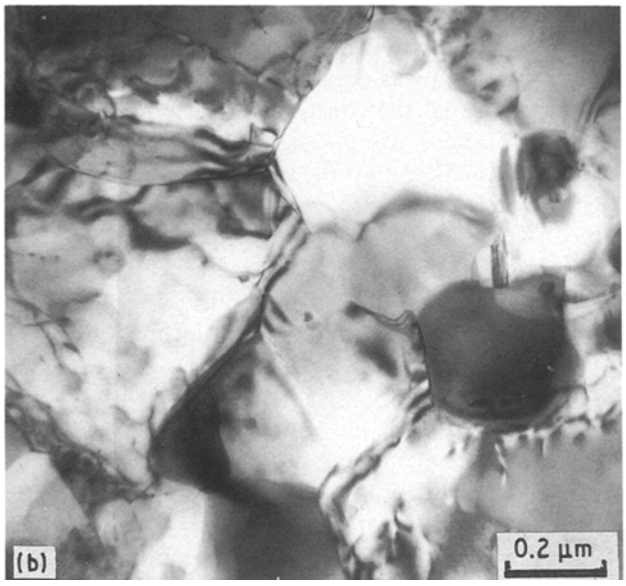

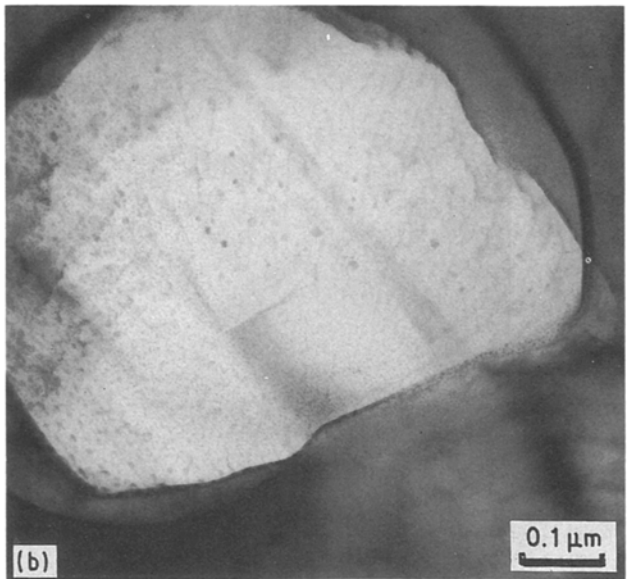

Figure 9 Microstructures developed at the temperature of 400 °C, surface equivalent strain rate of 0.083 s^{-1} and strain of 0.068: (a) worked structure, and (b) developing subgrain structure.

boundaries were composed of loose dislocation arrays, many of which interacted with particles (Fig. 9b). It appeared that the formation of the subgrain boundaries by integrating the loose, orderly dislocation arrays was retarded. The existence of the dislocations in undeveloped/developing subgrains indicates that the dynamic recovery was not prevalent, leading to the continuation of work-hardening. Dynamically recrystallized grains were not observed, as expected at this stage of deformation.

After deformation to the strain of $\varepsilon = 0.136$, being approximately at the stress peak, grains were elongated to a great extent, within which ill-defined equiaxed subgrains were developed (Fig. 10a). This is an important feature of the microstructure having evolved at this stage. Many of the subgrains contained a large number of dislocations, their sizes appeared to be independent of the interspacing of particles, and their boundaries were not at all clear. This indicates that

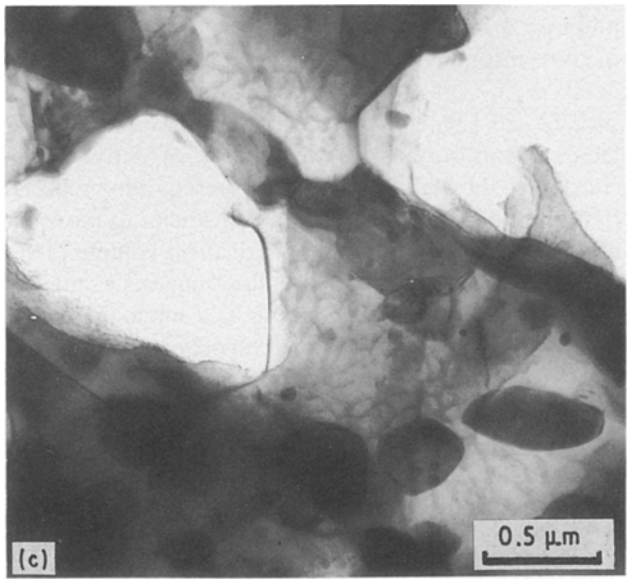

Figure 10 Microstructures developed at the temperature of 400 °C, surface equivalent strain rate of 0.083 s^{-1} and strain of 0.136: (a) elongated grain structure with subgrains; (b) equiaxed grain; (c) duplex structure.

although the strain rate was low, the dynamic recovery only proceeded to a limited extent, which encouraged dynamic recrystallization to occur. In the regions populated with fine particles, the nucleation of recrystallized grains was suppressed. Only in the particle-depleted regions, were equiaxed grains observed, as illustrated in Fig. 10b. As these grains contained an ill-defined substructure, they probably formed and grew before the ceasing of the deformation. The present observation appears to confirm a previous finding that dynamic recrystallization starts before the attainment of the stress peak [41]. As a consequence of the occurrence of recrystallization, a duplex microstructure, consisting of heavily worked grains and equiaxed new grains, was observed in some regions, as shown in Fig. 10c. In general, the volume fraction of this kind of recrystallized grains in the field examined was very low. At this strain rate, the temperature rise might be negligible. Coarsening of the constituent phases, which has been considered as the third possible effect causing the observed softening over the stress peak, was not visible, probably due to the existence of a spectrum of sizes of the multi-phase particles. The softening beyond the stress peak may thus be attributed largely to the occurrence of recrystallization. The low volume fraction of recrystallized grains is in agreement with the small degree of softening under this deformation condition, see Fig. 1a.

During the steady-state deformation (at the strain $\varepsilon = 0.45$), the balance between dynamic recovery and work hardening mainly governed the flow behaviour of the material. The balanced dislocation density was found to be dependent upon local particle density in the subgrains. In the regions with fewer particles, dislocation density in the subgrains was relatively low, which indicates that generated dislocations were annihilated by joining relatively stable dislocation arrays such as subgrain and grain boundaries. In the regions with many particles, the regularity of the subgrains was low and internal dislocation density remained high, as typically shown in Fig. 11a. At this stage, the recrystallized grains were subjected to continuing deformation, and therefore the overall microstructure had a worked appearance. A few newly formed, growing recrystallized grains contained irregular dislocations, as can be seen in Fig. 11b. It is therefore clear that at the low strain rate, the principal processes occurring in the material, accompanying external deformation, were dislocation generation and subgrain formation, which eventually led to a balance between work-hardening and softening, while dynamic recrystallization occurred only to a limited extent, which corresponds well with the shape of the stress–strain curve exhibited by the material under the given condition.

3.4.2. High strain rate ($2.49\ s^{-1}$)

The microstructural development at 400 °C and the strain rate of $2.49\ s^{-1}$ (which is 30 times as high as that discussed above) is of more interest, because this condition is more in agreement with that encountered in real metal forming. Owing to the brittleness of the material, the steady-state deformation was not attainable under this condition. And, owing to the very high twist speed ($5.5\ rev\ s^{-1}$), it was extremely difficult to interrupt the deformation exactly at the stress peak. Discussed below are the microstructures developed in deformation to the strains around the stress peak.

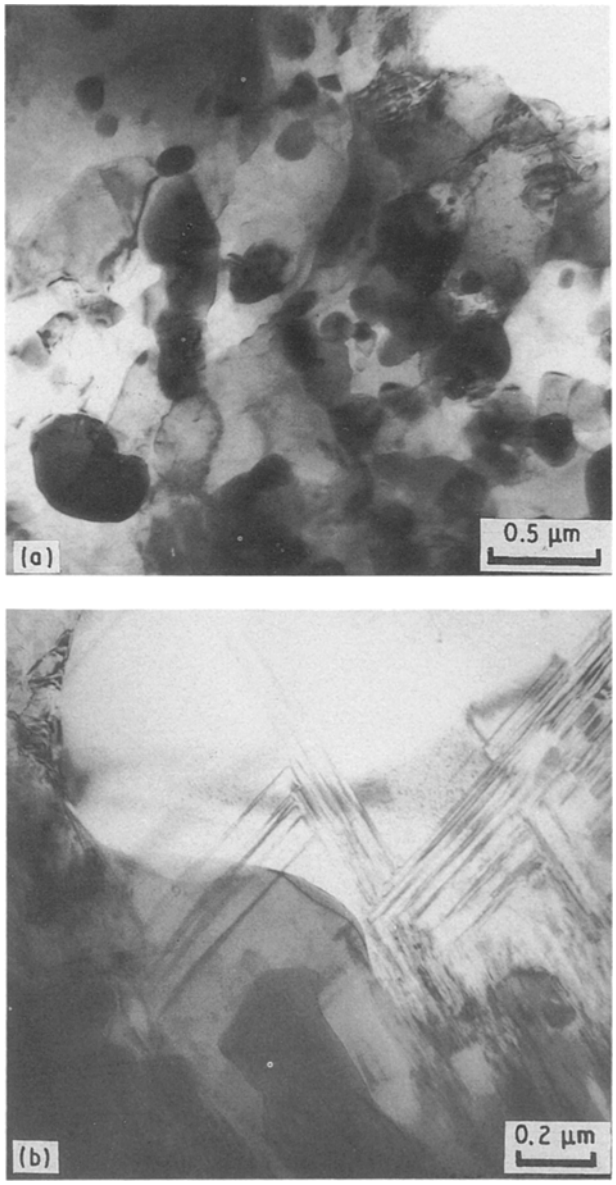

Figure 11 Microstructures developed at the temperature of 400 °C, surface equivalent strain rate of $0.083\ s^{-1}$ and strain of 0.45: (a) worked structure; (b) growth of a new grain with new dislocations.

Deformation to the strain $\varepsilon = 0.086$, which is in the work-hardening regime but very close to the stress peak, brought about the elongation of grains and formation of subgrains (Fig. 12a). The completion of the subgrain formation was again retarded by the particles. Fig. 12b clearly illustrates the residence of particles at 120° triple junctions of the subgrains. Low contrast suggests small misorientations between neighbouring subgrains. At this stage of deformation, the subgrain boundaries were still rather jagged, being composed of loose dislocation arrays, indicating that perfection of a subgrain structure was difficult to attain. As a result of the interactions between dislocations and particles, most of the subgrains were not

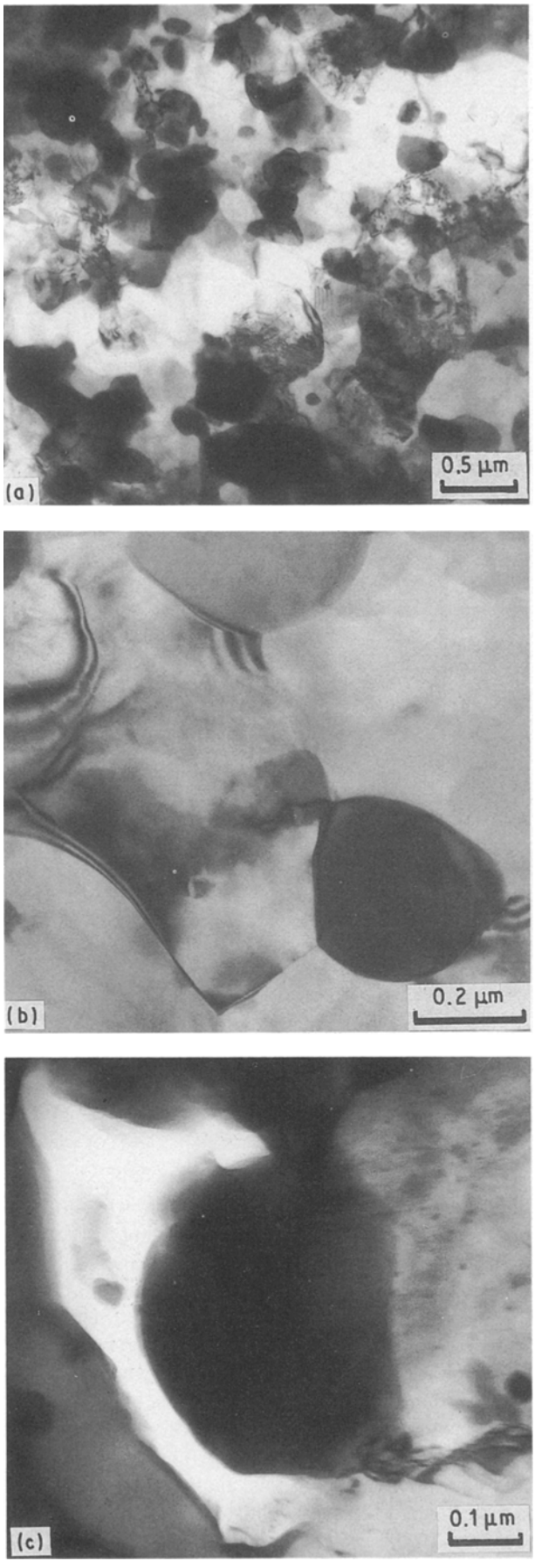

Figure 12 Microstructures developed at the temperature of 400 °C, surface equivalent strain rate of 2.49 s^{-1} and strain of 0.086: (a) general structure; (b) interaction between particles and subgrain boundaries; (c) outcrop of recrystallization at a particle.

well defined, not as regular as shown in Fig. 12b, but outlined by unclear subgrain boundaries. At this strain rate, the rate of dislocation generation was very high and could not be efficiently balanced with that of dynamic recovery and thus led to a very high degree of work hardening. The imbalance in strain-energy generation and relief provided a favourable condition for dynamic recrystallization to occur.

The evidence of dynamic recrystallization has been shown in the microstructure worked at the low strain rate. Of interest is the initiation of dynamic recrystallization during the deformation prior to the stress peak, which is of great importance in determining the nucleation mechanism. In the aluminium alloy (Al–5Mg–0.8Mn) containing Al_6Mn particles and having been torsion tested, equiaxed grains were observed but their nucleation sites could not be found. This was also the case for other materials like copper, stainless steel and nickel [14, 42]. However, it is known that dynamic recrystallization can be stimulated in the vicinities of particles with a relatively large size (usually larger than 1 μm for a deformed aluminium alloy during annealing) [43], due to local strain concentrations. Fig. 12c shows an example of the microstructure close to a particle with a size of 0.5 μm (smaller than the usual critical size for the static annealing process) in the deformed material. High-angle misorientation, as indicated by sharp contrast, suggests that this is an outcrop of a recrystallized grain, behind whose boundary a dislocation-free zone is growing into its deformed surroundings. Considering the high quenching capacity of the torsion machine used, it can be concluded that this grain was dynamically formed just before the deformation was interrupted. The observation of the recrystallization nucleation in the material worked at this stage again confirms that dynamic recrystallization starts at a strain lower than that to the stress peak [41]. This micrograph gives evidence not only that dynamic recrystallization is indeed stimulated by the particles, but also that the critical size of the particles which are capable of stimulating recrystallization, is shifted to a smaller value in the dynamic process with a high strain rate. It should be pointed out that the shift of the critical size for stimulating recrystallization does not mean that dynamic recrystallization must be initiated at all the particles larger than this size. On the contrary, the observed new grains were far fewer in number than these particles. The reason is that the initiation of recrystallization was effectively retarded by the finer particles surrounding the large ones.

Further deformation to the strain $\varepsilon = 0.19$, which is beyond the stress peak, did not produce a large difference in the microstructure of worked grains. Most of them contained an irregular substructure. Fig. 13a represents the general microstructure of the material worked at this stage. However, in the vicinity of the occasionally found original powder particle boundaries, retained in the material processed from the air-atomized powder, the irregularity was substantially lessened, appearing as a region with uniform dislocation networks, as shown in Fig. 13b. It is highly likely that in the vicinity of the boundary, recrystallization

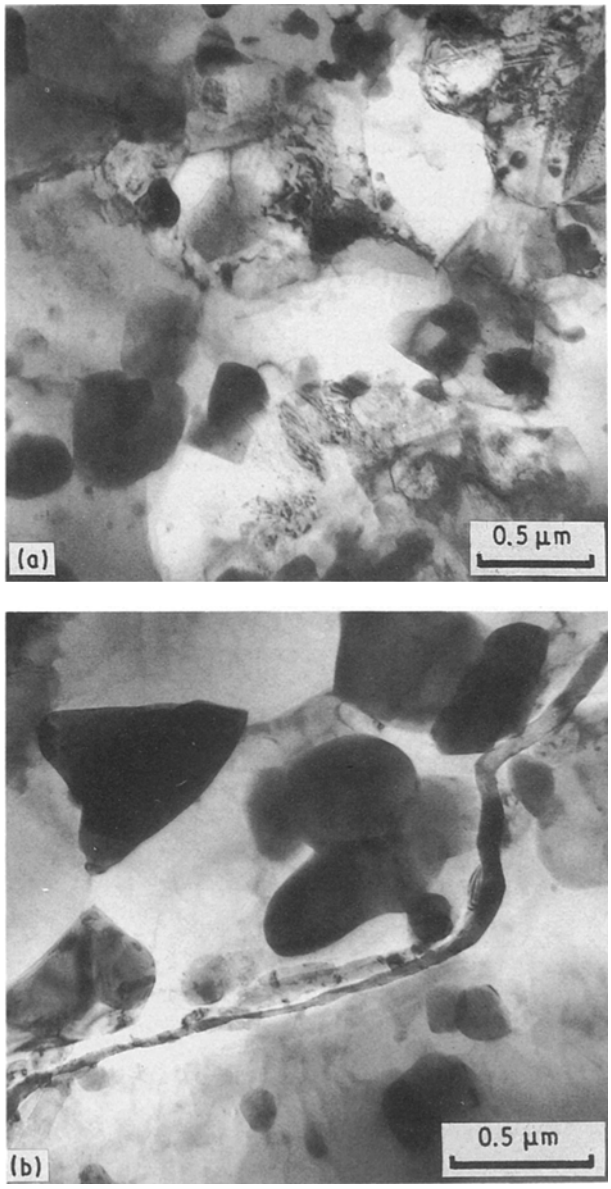

Figure 13 Microstructures developed at the temperature of 400 °C, surface equivalent strain rate of 2.49 s^{-1} and strain of 0.19: (a) worked structure; (b) structure near a retained original powder particle boundary.

occurred, thereby sweeping off the irregular dislocation tangles generated before the stress peak was attained. Hence, the image shown in Fig. 13b is likely a rebuilt microstructure. This is understandable because, to maintain structural continuity during deformation, the internal boundaries are the sites of strain concentrations and nucleation of new grains. Moreover, evidence of dynamic recrystallization near the original powder particle boundaries has also been found in the as-extruded material [8].

In general, there was much evidence that dynamic recrystallization was involved in the softening of the material and the volume fraction of the recrystallized grains was increased when compared with that in the material deformed at a lower strain rate. But its volume fraction was still low, making it difficult to believe that a low volume fraction of dynamic recrystallization alone could produce the large degree of softening, as shown in Fig. 1a. As the material worked under this condition failed during softening before attaining the steady-state deformation, the cracking of large dispersed-phase particles and initiation of the decohesion at the interfaces between the large dispersed-phase particles and aluminium matrix, both of which would result in a stress relief, may also be responsible. Additionally, at the high strain rate, a temperature rise would be another contributor to the softening.

4. Conclusions

1. The hot-working behaviour of the Al–20Si–7.5Ni–3Cu–1Mg alloy differed from that of conventional aluminium alloys by exhibiting a distinct stress peak in the stress–strain curves during torsional deformation. The stress peak appears to be caused by a combination of several effects, mainly by local dynamic recrystallization.

2. The ductility of the material was generally very low in comparison with conventional aluminium alloys, particularly at low temperatures and high strain rates. Special caution should, therefore, be taken in choosing deformation conditions to prevent cracking during deformation.

3. A high strain rate sensitivity, m, of the material was found. A constitutive Equation 7 for steady-state deformation has been used to explain the finding, which shows that the high m values are mainly associated with a high activation energy for deformation. As the stress of the material is much more deformation rate dependent than that of conventional aluminium alloys, attention should be paid to the adjustment of deformation parameters to be applied.

4. The m value of the material was shown to vary greatly with temperature, which could not be explained with Equation 7. This suggests that additional factors specific to technical alloys should be considered, such as parameters of second-phase particles whose influence on dislocation velocity (deformation rate) is temperature dependent. The increase of m with temperature indicates that it is more effective to reduce the stress by lowering deformation rate at a higher temperature.

5. Temperature had a profound effect on the stress of the material. This effect, together with that of strain rate, has been described with a hyperbolic sine constitutive equation with constitutive constants different from those of conventional aluminium alloys. The activation energy for deformation was found to be much higher than that of pure aluminium, probably arising from a high volume fraction of multi-phase particles as additional barriers to metal flow.

6. At 400 °C and 0.083 s^{-1}, deformation mainly proceeded by the interaction between work hardening and softening by dynamic recovery. However, dynamically recrystallized grains were also found in the material strained to the stress peak, which confirms the role of recrystallization in resulting in the softening following the stress peak.

7. An increased strain rate of 2.49 s^{-1} promoted the nucleation of recrystallization in the vicinity of dispersed particles with sizes smaller than 1 μm. But the

volume fraction of recrystallized grains remained low, which suggests that other effects also played roles in leading to the large softening beyond the stress peak.

Acknowledgements

The authors thank the Showa Denko K. K., Japan, for supplying the powder used as the raw material in this work, and Professor L. Delaey and Mr G. Herbots, Katholieke Universiteit Leuven, Belgium, for the provision of the experimental facilities and for the assistance with the torsion tests, respectively. Financial support from the Programme of Innovative Research (IOP), the Netherlands, is gratefully acknowledged.

References

1. "PM and Spray Deposition of Al–Si–Fe–2Ni Alloy", *Metal Powder Report* **45** (1990) 403.
2. P. SMITH, *Powder Metall.* **33** (1990) 202.
3. J. ZHOU and J. DUSZCZYK, *J. Mater. Shaping Technol.* **6** (1989) 241.
4. J. ZHOU, J. DUSZCZYK and B. M. KOREVAAR, *ibid.* **8** (1990) 91.
5. *Idem*, in "Advanced Technology of Plasticity 1990", Proceedings of the 3rd International Conference on Technology of Plasticity, Kyoto, Japan, July 1990, Vol. 2 (Japan Society for Technology of Plasticity, Tokyo, 1990) p. 957.
6. H. SANO, M. ABO and S. YAMAUCHI, *Sumitomo Light Metal Tech. Rep.* **30** (1989) 24.
7. Y. HIRAI, K. KANAYAMA, M. NAKAMURA, H. SANO and K. KUBO, *Aluminium* **66** (1990) 389.
8. J. ZHOU, J. DUSZCZYK and B. M. KOREVAAR, *J. Mater. Sci.* **27** (1992) 3.
9. *Idem, ibid.* **27** (1992) 3.
10. B. VERLINDEN, *ATB Metall.* **29** (3, 4) (1989) 39.
11. M. J. LUTON, in "Workability Testing Techniques", edited by G. E. Dieter (ASM, Metals Park, OH, 1984) p. 95.
12. J. Z. GRONOSTAJSKI and H. H. ZIEMBA, *Metal Sci.* **16** (1982) 405.
13. M. E. KASSNER, M. M. MYSHLYAEV and H. J. McQUEEN, *Mater. Sci. Engng* **108A** (1989) 45.
14. H. J. McQUEEN, E. EVANGELISTA, J. BOWLES and G. CRAWFORD, *Metal Sci.* **18** (1984) 395.
15. R. ØRSUND and E. NES, in "Annealing Processes–Recovery, Recrystallization and Grain Growth", Proceedings of the 7th Risø International Symposium on Metallurgy and Materials Science, Roskilde, Denmark, September 1986, edited by N. Hansen, D. Juul Jensen, T. Leffers and B. Ralph (Risø National Laboratory, Roskilde, 1986) p. 475.
16. B. VERLINDEN, P. WOUTERS, H. J. McQUEEN, E. AERNOUDT, L. DELAEY and S. CAUWENBERG, *Mater. Sci. Engng* **123A** (1990) 229.
17. P. WOUTERS, B. VERLINDEN, H. J. McQUEEN, E. AERNOUDT, L. DELAEY and S. CAUWENBERG, *ibid.* **123A** (1990) 239.
18. L. F. MONLDOFO, "Aluminium Alloys, Structure and Properties" (Butterworths, London, 1976) pp. 509, 566, 604.
19. H. L. YIU and T. SHEPPARD, *Mater. Sci. Technol.* **1** (1985) 209.
20. E. EVANGELISTA, P. MENGUCCI, E. DI RUSSO, P. FIORINI and H. J. McQUEEN, in "Proceedings of the 8th International Light Metals Congress", Leoben, Vienna, Austria, June 1987, edited by F. Jeglitsch (Aluminium-Verlag, Düsseldorf, 1987) p. 544.
21. J. ZHOU and J. DUSZCZYK, *J. Mater. Sci.* **25** (1990) 4541.
22. A. ALTAN, O. OH and H. GEGEL, "Metal Forming, Fundamentals and Applications" (ASM, Metals Park, OH, 1983) p. 65.
23. M. Y. WU and O. D. SHERBY, *Scripta Metall.* **18** (1984) 773.
24. C. H. HAMILTON and A. K. GHOSH, *Metall. Trans.* **11A** (1980) 1494.
25. D. W. CHUNG and J. R. CAHOON, *Metal Sci.* **13** (1979) 635.
26. "Advanced P/M Aluminium Alloys for High-Performance Applications", private communication, Technical Research Laboratories, Sumitomo Light Metal Industries, Ltd, Nagoya, Japan, June 1989.
27. K. CONROD and H. J. McQUEEN, in "Proceedings of the International Conference on Aluminium Alloys, their Physical and Mechanical Properties", Charlottesville, VA, USA, June 1986, edited by E. A. Starke Jr and T. H. Sanders Jr, Vol. 1 (Engineering Materials Advisory Services, Warley, UK, 1986) p. 435.
28. R. A. AYRES, *Metall. Trans.* **8A** (1977) 487.
29. T. H. ALDEN, *Acta Metall.* **37** (1989) 1683.
30. I. SZKRUMELAK, K. CONROD and H. J. McQUEEN, in "Proceedings of the 8th International Light Metals Congress", Leoben, Vienna, Austria, June 1987, edited by F. Jeglitsch (Aluminium-Verlag, Düsseldorf, 1987) p. 539.
31. W. A. WONG and J. J. JONAS, *Trans. Metall. Soc. AIME* **242** (1968) 2271.
32. O. D. SHERBY, R. H. KLUNDT and A. K. MILLER, *Metall. Trans.* **8A** (1987) 843.
33. J. R. PICKENS, T. J. LANGAN, R. O. ENGLAND and M. LIEBSON, *ibid.* **18A** (1987) 303.
34. P. OLLA and P. F. VIRDIS, *ibid.* **18A** (1987) 293.
35. G. AVRAMOVIC-CINGARA, H. J. McQUEEN, A. SALAMA and T. R. McNELLEY, *Scripta Metall.* **23** (1989) 273.
36. A. ESPEDAL, H. GJESTLAND, N. RYUM and H. J. McQUEEN, *Scand. J. Metall.* **18** (1989) 131.
37. K. P. RAO and Y. V. R. K. PRASAD, *Aluminium* **60** (1984) 184.
38. J. A. BAILEY, S. L. HAAS and M. K. SHAH, *Int. J. Mech. Sci.* **14** (1972) 735.
39. T. SHEPPARD, in "Extrusion, Scientific and Technical Developments", edited by G. Lang, A. F. Castle, M. Bauser and G. Scharf (Deutsche Gesellschaft für Metallkunde, Oberursel, 1981) p. 17.
40. J. J. JONAS, C. M. SELLARS and W. J. McG. TEGART, *Int. Metall. Rev.* **14** (1969) 1.
41. H. J. McQUEEN and J. J. JONAS, in "Plastic Deformation of Materials, Treatise on Materials Science and Technology", edited by R. J. Arsenault, Vol. 6 (Academic Press, New York, 1975) p. 393.
42. E. EVANGELISTA, H. J. McQUEEN and E. BONETTI, in "Deformation of Multi-Phase and Particle Containing Materials", Proceedings of the 4th Risø International Symposium on Metallurgy and Materials Science, Roskilde, Denmark, September 1983, edited by J. B. Bilde-Sørensen, N. Hansen, A. Horsewell, T. Leffers and H. Lilholt (Risø National Laboratory, Roskilde, 1986) p. 243.
43. H. M. CHAN and F. J. HUMPHREY, *Acta Metall.* **32** (1984) 235.

Received 3 June
and accepted 10 September 1991